In vivo imaging of elastic fibers using sulforhodamine B

Clément Ricard
INSERM, U836
Grenoble Institut des Neurosciences
Grenoble, F-38042 France
and
Université Joseph Fourier
BP 53
Grenoble Cedex 9, F38041 France

Jean-Claude Vial
Julien Douady
CNRS UMR 5588
Laboratoire de Spectrométrie Physique
Saint Martin d'Hères, F-38042 France
and
Université Joseph Fourier
BP 53
Grenoble Cedex 9, F-38041 France

Boudewijn van der Sanden
INSERM, U836
Grenoble Institut des Neurosciences
Grenoble, F-38042 France
and
Université Joseph Fourier
BP 53
Grenoble Cedex 9, F38041 France

Abstract. Until now, the imaging of elastic fibers was restricted to tissue sections using the endofluorescence properties of elastin or histological dyes. Methods to study their morphology *in vivo* and *in situ* have been lacking. We present and characterize a new application of a fluorescent dye for two-photon microscopy: sulforhodamine B (SRB), which is shown to specifically stain elastic fibers *in vivo*. SRB staining of elastic fibers is demonstrated to be better than using elastin endofluorescence for two-photon microscopy. Our imaging method of elastic fibers is shown to be suitable for simultaneous imaging with both other fluorescent intravital dyes and second-harmonic generation (SHG). We illustrate these findings with intravital imaging of elastic and collagen fibers in muscle epimysium and endomysium and in blood vessel walls. We expect SRB staining to become a key method to study elastic fibers *in vivo*. [DOI: 10.1117/1.2821421]

Keywords: intravital multiphoton microscopy; elastic fibers; collagen fibers; sulforhodamine B; second-harmonic generation.

Paper 07069R received Feb. 28, 2007; revised manuscript received Jul. 4, 2007; accepted for publication Aug. 3, 2007; published online Dec. 18, 2007.

1 Introduction

Elastic fibers are an essential structure of the extracellular matrix (ECM). They are composed of two main components: an amorphous core of elastin, which is a hydrophobic protein, surrounded by a mantle of fibrillin-rich microfibrils.[1–4]

These elastic fibers are responsible for the long-range deformability of blood vessels and lung tissue and the passive recoil of connective tissues. Further, they are often present in ligaments and skin as well as in dynamic connective tissues, such as in muscle epimysium (connective tissue surrounding muscle) and endomysium (connective tissue in between muscle fibers). They are responsible for the resilience of these tissues, whereas collagen fibrils are responsible for their tensile strength.[1,5] Due to their small sizes, intravital imaging of elastic fibers requires the utilization of nonlinear optical methods.

Intravital multiphoton microscopy has emerged during the past 10 years as an innovative method to investigate anatomical, physiological, and pathophysiological features directly *in vivo* with a micrometric spatial resolution and an enhanced imaging depth (for review see Refs. 6 and 7). It was successfully applied to the study of, for instance: the brain microvasculature of mice up to 600 μm below the dura,[8] neuronal activity,[9] or muscular caspase activity using transgenic mice.[10]

A large set of intravital dyes were designed and tested to stain biological structures of interest in multiphoton microscopy.[11] For example, intravenous injections of FITC or rhodamine-dextran molecules were used to study the brain microvasculature.[12,13] Intravenous injection of a cocktail of Hoechst 33342 and propidium iodide was used to assess cell death after an ischemia in kidneys.[14] More recently, the direct injection of sulforhodamine 101 in brain was unveiled as a method for specifically staining astrocytes.[15]

Histological staining of elastic fibers using the Weigert or the resorcin-fuschsin methods[1,16] are incompatible with intravital studies.

More recently, the acquisition of elastin endofluorescence signal using two-photon excited fluorescence (2PEF) was demonstrated on *ex vivo* slices of rat aortas but with a limited imaging depth (50 μm) and a long acquisition time[17] (5 s); these characteristics are not suitable for intravital experiments.

We found a new utilization of a classic dye that appears to be specific to elastic fibers. Its high two-photon quantum yield now enables the observation of these fibers directly *in vivo* in real physiological conditions. Two modes of administration have been successfully tested: intravascular injection and intissue diffusion after droplet deposit. The knowledge arising from these observations would be of particular interest in, e.g., studying blood vessel[18] responses after the administration of vasoactive drugs and tumor invasive growth that depend on collagen and elastic fibers in the ECM (Ref. 19).

Address all correspondence to Clement Ricard, Grenoble Institute des Neurosciences (GIN), Centre de Recherche INSERM U 836 UJF-CEA-CHU, Equipe: Neuroimagerie Fontctionnelle et Métabolique, Chemin Fortuné Ferrini, Université Joseph Fourior - site Santé, BP 170 La Tronche, 38042 Grenoble cedex 9, France; Tel: +33 4 56 52 06 17; Fax: +33 4 56 52 05 98; E-Mail: Clement.Ricard@ujf-grenoble.fr

1083-3668/2007/12(6)/064017/8/$25.00 © 2007 SPIE

In addition, with a specific microscopic setup, it is possible to observe simultaneously 2PEF of intravital dyes and second-harmonic generation (SHG) signals. The SHG signal was demonstrated to be specific of certain types of collagen[20] (e.g., types I and III) and myosin in muscle fibers, however, elastic fibers do not exhibit any SHG signal.[21] These characteristics enable the simultaneous observation of both elastic and collagen fibers without any crosstalk.

The aim of this study is to present a new application of a fluorescent dye: the sulforhodamine B (SRB), for imaging elastic fibers *in vivo*. First, SRB staining of elastic fibers is demonstrated to be better than using elastin endofluorescence for two-photon microscopy. Then, elastic fiber imaging is shown to be suitable for simultaneous imaging with both other fluorescent intravital dyes and SHG. We illustrate these findings with intravital imaging of elastic and collagen fibers in muscle epimysium and endomysium, and in blood vessel walls.

2 Methods

2.1 *Animal Care Guidelines*

All experimental procedures were performed in accordance with the French Government guidelines for the care and use of laboratory animals (licenses 380702, A 3851610004, and B 3851610003). Twenty healthy female nude mice and three healthy female Wistar rats (Charles River Laboratories, France) were used in the experiments.

2.2 *Animal Preparation*

Mice were anesthetized by a continuous inhalation of 1.5% isoflurane in a gas mixture of 30% O_2 and 70% N_2O, and placed on a stereotaxic frame modified to enable anterior-posterior rotation of the animal to optimize laser penetration. Core temperature was maintained at approximately 37 °C using warm water circulating through a pad.

For muscle studies, the hindlimb of the mouse was blocked in a homemade restraint to reduce the movements caused by the animal respiration. A small piece of skin (4 to 5 mm in diameter) was removed above the muscle or above the femoral artery, depending on the experiment. The exposed area was filled with a 0.9% saline water solution and the injection of the dye occurred at approximately 10 min after surgery.

2.3 *Dye Preparation*

For the SRB and SHG experiments, 50 μl of a 10-mg/ml SRB (Lambda Physics) in 0.9% saline water solution was injected in the tail vein of the mouse approximately 10 min before the two-photon microscopy studies.

For double-staining experiments a cocktail of 50 μl of a 10-mg/ml SRB solution and of 100 μl of a 100-mg/ml FITC-dextran 70-kDa solution (Sigma-Aldrich) in 0.9% NaCl was prepared.

2.4 *Microscopy Setup*

Two-photon laser scanning microscopy was performed with a confocal microscope consisting of a Biorad MRC 1024 scanhead and an Olympus BX50WI microscope. Both fluorescence and SHG signals were directly epicollected, as shown in Fig. 1(a). An 800-nm excitation beam from a Tsunami femtosecond Ti:sapphire laser (5-W pump; Spectra-Physics, Millenia V) was focused in the sample using a 20× water-immersion objective [0.95 numerical aperture (NA), Xlum Plan Fl Olympus]. The pulse length at the entrance of the microscope is 100 fs, but the light is strongly dispersed, mainly by the lenses of the objective. Therefore, we estimate a 500-fs length at the focal plane.

The beam was scanned in the *x-y* plane to acquire 512 ×512-pixel images in 0.9 s. The *z* scan for variation of the observation depth was realized by vertical motion of the motorized objective. The incident laser intensity was adjusted by using a half-wave plate and a polarizer placed before the microscope so that the total average power delivered at the surface ranged from 1 to 150 mW. Two channels could be simultaneously observed using two added external photomultiplicator tubes (PMTs) and appropriate filters, as shown in Fig. 1(a). During our experiments, three different filter sets were applied [see Figs. 1(c)–1(e)]. Images were acquired using the Biorad exploitation system and displayed using ImageJ (ImageJ. v.1.33 Public Domain Software, available at http://rsb.info.nih.gov/ij/, 2005).

2.5 *Fluorescence Spectrum*

A 0.9% saline water solution of SRB in a glass vial was excited by two-photon transition by the focused TiSa laser at 800 nm. The fluorescence collected at a right angle was analyzed by a spectrophotometer (Jobin Yvon H-20).

2.6 *SRB Quantum Yield*

The absolute measurement of the quantum yield is difficult. Therefore, a relative quantum yield was determined.[23] The fluorescence efficiency of an unknown molecule is related to a standard dye using the equation

$$\phi_{F(x)} = \frac{A_s}{A_x}\frac{F_x}{F_s}\left(\frac{n_x}{n_s}\right)^2 \phi_{F(s)},$$

where Φ is the fluorescence quantum yield, A is the absorbance at the excitation wavelength, F is the area under the corrected emission curve (expressed in number of photons), and n is the refractive index of the solvents used. Subscripts s and x refer to the standard dye and to the unknown molecule, respectively.

In this equation, absorbance A accounts for the number of absorbed photons and area F accounts for the number of emitted photons. In the present experiment, $n_x/n_s = 0.98$.

The 0.9% saline water solution of SRB fluorescence quantum yield was then measured relative to rhodamine 101 solution in ethanol as standard. The quantum yield for rhodamine 101 was taken as unity.[24]

2.7 *Laser Power Measurements*

The power was measured at the output of the objective (i.e., at the surface of the tissue) using a calibrated calorimetric power meter (Coherent Inc. model 205), it was chosen for its large sensitive area (3 cm^2) to collect all the light coming out of the objective.

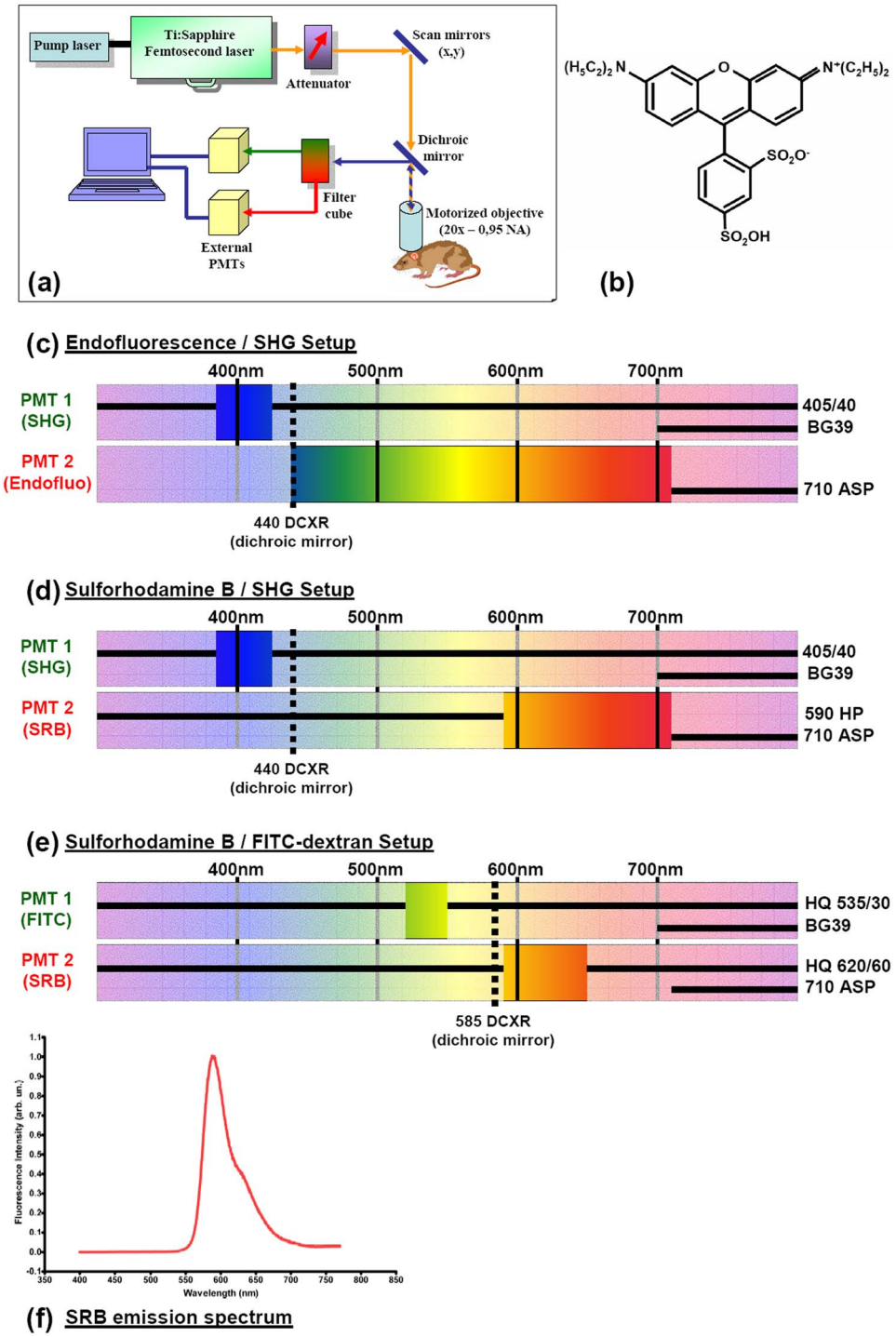

Fig. 1 Experimental conditions: (a) microscopy setup used in all of our experiments, (b) chemical structure of the SRB molecule, and (c) to (e) the three filter sets used in our study with the corresponding wavelengths observed (c) the endofluorescence/SHG setup, (d) the SRB/SHG setup, and (e) the SRB/FITC-dextran setup. Horizontal black lines correspond to the blocked light. Vertical dotted lines represent the transition wavelengths of the dichroic mirrors. (f) SRB emission spectra under a two-photon excitation at 800 nm. Two-photon excitation spectrum is described in Ref. 22. The rhodamine B spectrum can be used as a reference as the fluorescence moieties are identical for SRB and rhodamine B.

2.8 *Immunohistochemistry*

Thoracic aortas were taken on Wistar rats (Charles River Laboratories, France) and fixed in a 4% paraformaldehyde solution. Then 1-mm thin aorta rings were cut and washed in phosphate-buffered saline (PBS, Sigma). The rings were incubated for 4 h at 20 °C with a mouse monoclonal antielastin antibody (1/100 in PBS-bovine serum albumin 3%—Abcam BA-4). Then, they were incubated for 2 h at 20 °C with a FITC donkey antimouse secondary antibody (1/100, Jackson Immunoresearch). Finally, the rings were incubated for 5 min

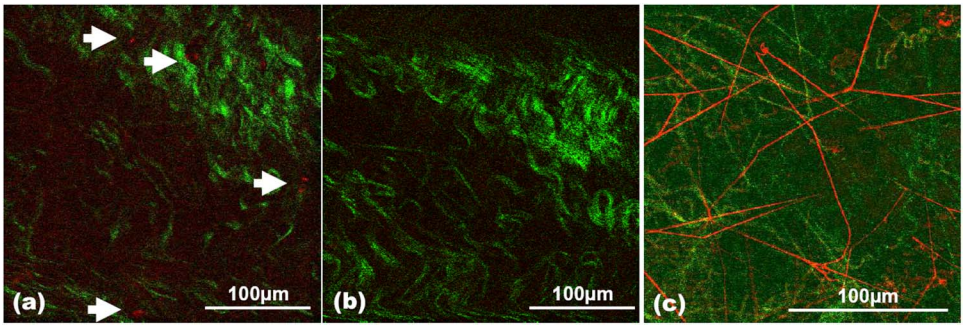

Fig. 2 Comparison between endofluorescence and SRB staining of elastic fibers: (a) merge of endofluorescence (red, PMT2) and SHG (green, PMT1) imaging of muscle epimysium using the endofluorescence/SHG setup, note the staining of some cells on PMT2 (arrows) due to the fluorescence of endogenous biomolecules;[11] (b) merge of endofluorescence (red, PMT2) and SHG (green, PMT1) imaging of muscle epimysium using the SRB/SHG setup; and (c) merge of SRB 2PEF (red, PMT2) and SHG (green, PMT1) imaging of muscle epimysium using the SRB/SHG setup, 10 min after the intravenous injection of SRB. In the SRB image, a rolling ball background subtraction with a radius of 10 pixels was applied. All of theses images were acquired using an 800-nm excitation wavelength, with a 60-mW incident laser power. The acquisition time was 0.9 s/image. (Color online only.)

in a 0.5-mg/ml SRB solution and were washed five times before observation. Images were acquired using the microscopy setup already described with the filter set depicted in Fig. 1(e).

3 Results

3.1 *SRB Emission Spectrum and Quantum Yield*

The SRB emission spectrum shows a maximum peak at 590 nm, but no signal is detectable for wavelengths below 560 nm [see Fig. 1(f)]. This enables a simultaneous acquisition of light at lower wavelengths emitted by another dye or by SHG. The quantum yield of SRB is 80±10%.

3.2 *Comparison Between Endofluorescence and SRB Staining of Elastic Fibers*

To analyze the contribution of elastic fibers endofluorescence in the collected light, both 2PEF and SHG images of unstained living mice muscle epimysium with the endofluorescence/SHG setup were acquired [Fig. 2(a)]. SHG images of collagen fibers allow the correct positioning of the focal plane in the muscle epimysium.

With a 60-mW incident laser power during a 0.9-s acquisition time, it is impossible to observe any elastic fiber [Fig. 2(a)]. However, a weak fluorescence signal of endogenous biomolecules is present[11] [see arrows in Fig. 2(a)]. At the same depth, the SHG signal generated by collagen fibers is noticeable.

Under similar conditions but with the SRB/SHG setup, the fluorescence signal is no longer detectable [see Fig. 2(b)]. After the intravenous bolus injection of SRB, the characteristic pattern of elastic fibers in connective tissues slowly appears within minutes and reaches its maximum after approximately 10 min [Fig. 2(c)]. The simultaneous acquisition of both SHG and 2PEF signals [Fig. 2(c)] enables the nearly complete imaging of the connective tissue fibers.

The same experiment was performed with the deposit of a droplet of a SRB solution (0.5 mg/ml) directly on the muscle epimysium. After 5 min and eight washes with 0.9% saline water solution, we observed a similar staining.

This SRB staining is specific for the elastic fibers and was acquired in less than a second with a relatively low incident laser power: 25 mW are sufficient to exploit images. In conclusion, we demonstrated that these conditions are suitable for *in vivo* observations, which is not the case for endofluorescence imaging of elastic fibers.

3.3 *Double Staining*

As shown in Fig. 1(f), the spectral window below 560 nm is free; therefore it is possible to simultaneously use another intravital dye to study, e.g., both elastic fibers and the functional vasculature *in vivo*.

After the intravenous injection of a cocktail of SRB and FITC-dextran, two-photon images show elastic fibers in the epimysium [Fig. 3(a) (left)], in the endomysium around muscular fibers [Fig. 3(a) (asterisk)], and in blood vessel walls [Fig. 3(a) (arrow)], as well as the functional vascular network due to the staining of the blood plasma by FITC-dextran.

As seen previously, both SRB 2PEF and SHG signals have been acquired simultaneously and reveal the elastic and collagen fibers in the muscle epimysium [Fig. 3(b) (right)]. In addition, SHG signal results in a striped structure typical of myosin in skeletal muscle fibers [see Fig. 3(b) (left) and Fig. 3(c)].

3.4 *In vivo SRB Staining of Elastic Fibers in Arteries and Veins*

Large amounts of elastic fibers can be found in arteries and to a smaller extent in veins. The artery walls are composed of three different parts: (1) the intima, which is the closest part near the lumen, and whose is essentially made of endothelial cells; (2) the media, which layer is rich in elastic fibers and smooth muscle cells (SMCs); and (3) the adventia, which is composed of collagen and elastic fibers. The limit between the intima and the media is characterized by a thick layer of elastic fibers called internal elastic lamina. The limit between the media and the adventia is characterized by the external elastic lamina composed of elastic fibers with a fenestrated configuration.[25]

In this present study, the whole mouse femoral artery was

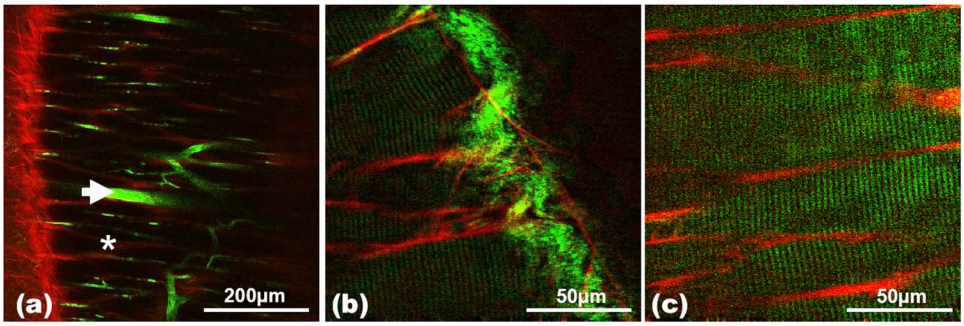

Fig. 3 Double staining: (a) two-photon image taken with the SRB/FITC-dextran filter set in the hindlimb muscle of a mouse at 10 min after the intravenous injection of a cocktail of SRB (red) and FITC-dextran (green). Note the presence of elastic fibers around blood vessels (arrow) and muscle fibers (asterisk). (b) and (c) merge of two images (SRB, red; SHG, green) taken with the SRB/SHG filters set-up in the muscle of a mouse at 10 min after the intravenous injection of SRB. SHG enables the observation of collagen fibers in the muscle epimysium (b, right) and myosin in the muscle fibers (b, left and c). SRB 2PEF shows elastic fibers in muscle epimysium and endomysium. All theses images were acquired at an 800-nm excitation wavelength, with a 60-mW incident laser power. The acquisition time was 0.9 s/image. (Color online only.)

imaged *in situ* using both SRB 2PEF and SHG with an incident laser power of 60 mW at 800 nm. Due to short-wavelength absorption, the SHG signal can be detected only on the first 50 μm. After computer reconstruction based on horizontal slices, we obtained cross sections of the artery at low magnification [see Fig. 4(a)] and high magnification [see Fig. 4(b)]. The internal and external elastic lamina are well defined and the darker area in between is the media.

Figures 4(c)–4(e) are horizontal slices taken at different depths [positions are defined in Fig. 4(b)]. The adventia [see Fig. 4(c)] is composed of collagen fibers (SHG signal in green) and elastic fibers (2PEF of SRB in red). In Fig. 4(d), the fenestrated structure of the external elastic lamina can be observed (bottom). Further, elastic fibers in the external elastic lamina are directly related to those in the adventia and beyond the adventia in adjacent connective tissue. Figure 4(e) enables the observation of the lumen of the artery and the internal and external elastic lamina. Elastic fibers are also observed in between the two lamina [see arrow in Fig. 4(e)] and SMC in the media which appear as dark holes [see asterisk in Fig. 4(e)]. SHG signals arising from the collagen fibers of the adventia are also visible [see Fig. 4(e) (top)].

The vein walls are also composed of three different layers (intima, media, and adventia). Unlike arteries, elastic fibers are less present and as a consequence, the media is thinner. Moreover, the internal elastic lamina is underdeveloped and the external elastic lamina is nonexistent.[25]

Figure 4(f) depicts a vein in the mouse hindlimb muscle. This image was taken *in vivo* after an intravenous SRB injection and shows a layer of elastic fibers with a highly fenestrated configuration. In comparison to an artery wall structure [Figs. 4(a)–4(e)], no other elastic layer was observed in this vein.

All results just described were similar after a local deposit of the SRB dye.

4 Discussion

Our experiments demonstrate that SRB specifically stains the elastic fibers and enables a direct *in vivo* observation with multiphoton microscopy. The microscopy setup shown in this paper enables the simultaneous observation of elastic fibers and other structures stained by other dyes (e.g., FITC-dextran staining of the blood plasma) or imaged by SHG of collagen or myosin.

4.1 *Biochemical Advantages of the SRB*

SRB is a low-molecular-weight (560 Da) polar fluorescent molecule with two sulfonic groups, making it highly hydrosoluble (solubility). The presence of two short alkylic arms and aromatic cycles makes it slightly lipophilic [see Fig. 1(b)], its octanol-water partition coefficient[26] is $\log K_{OW} = -0.45$. The molecule belongs to the xanthenes family, which contains many fluorescent dyes used for *in vivo* imaging (rhodamine 6G or sulforhodamine 101, for example[15,27,28]); some of them are already used in clinics (sodium-fluorescein[29]).

Until now, SRB was applied in cellular colorimetric assays because of its binding capability to basic amino acid residues under mildly acidic conditions.[30] More recently, it was reported as a marker to assess the blood-brain-barrier permeability.[13]

SRB was reported to have a very low toxicity (LD_{50}: 10,300 mg/kg for the mouse, Sigma-Aldrich MSDS). The dose (22 mg/kg) injected in the mice during our experiments is far below the lethal dose. Moreover, experiments have shown that the SRB does not bind to plasma albumin and that the complete clearance by the kidneys is within 180 min (unpublished data).

4.2 *Comparison with Endofluorescence Imaging of Elastic Fibers*

Recently, various authors have reported the endofluorescence properties of many biomolecules and their ability to be excited by two-photon excitation.

The 2PEF of the endofluorescence of elastin was reported at different IR excitation wavelengths [760 (Refs. 31–33), 800 (Ref. 34), and 860 nm (Refs. 17 and 35)]. In each case, the emission has a low efficiency in comparison with dye staining and is in the blue range that is highly scattered and absorbed by surrounding tissues.

As a consequence, the imaging of elastic fibers using endofluorescence properties of the elastin requires long exposure

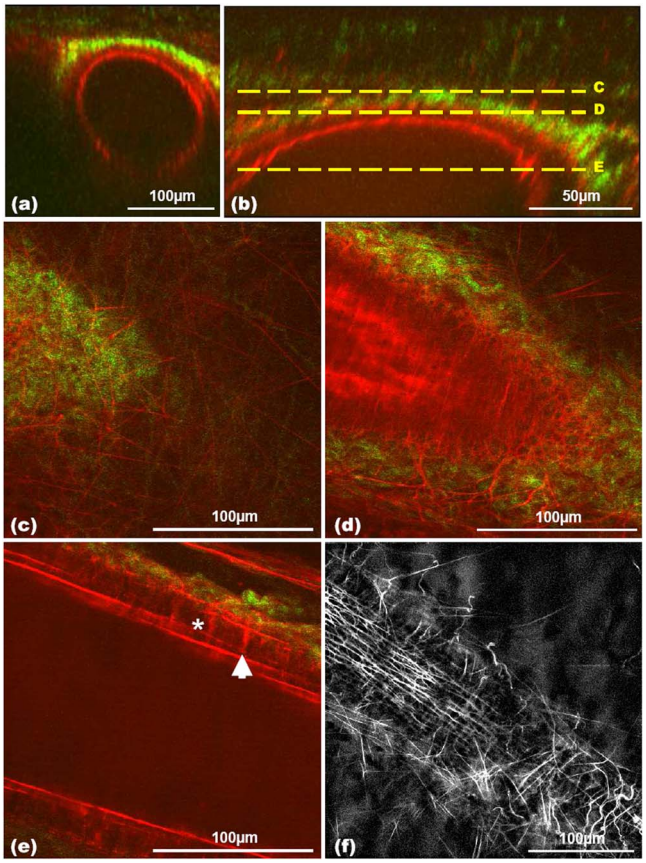

Fig. 4 SRB specifically stains elastic fibers around femoral artery and muscular veins with a micrometric resolution: (a) cross section of the femoral artery reconstituted from 84 slices acquired *in situ* at ~1 min after euthanasia of the animal (red, SRB 2PEF from elastic fibers; green, SHG signal from collagen); (b) higher magnification of (a) showing the depth of the different horizontal slices displayed in (c), (d), and (e) (dashed lines), the origin ($z=0$) is taken at the surface of connective tissue surrounding the artery; (c) horizontal slice ($z=41$ μm) in the adventia (notice the presence of collagen in green); (d) horizontal slice ($z=53$ μm) in the media (notice the fenestrated structure of elastic fibers at the bottom of the picture, which is characteristic for the external elastic layer); (e) horizontal slice ($z=73$ μm) in the lumen of artery [notice the internal elastic layer and elastic fibers between the internal elastic layer and the adventice (arrow), dark holes in the media (asterisk) are the smooth muscle cells]; and (f) horizontal slice taken *in vivo* in the media of a muscular vein. Note the absence of an external elastic lamina and the highly fenestrated internal elastic lamina. All theses images were acquired at an 800-nm excitation wavelength, with a 60-mW incident laser power. The acquisition time was 0.9 s/image. (Color online only.)

times,[17] above 5 s at 860 nm. These delays are not compatible with intravital studies due to the respiratory movements of the animal and a laser power increase is not relevant due to possible tissue damage. Moreover, the imaging depth is limited (to 50 μm, Ref. 17), which also makes it of less interest for intravital studies.

In addition, other biomolecules such as riboflavins or NAD(P)H are also excited,[11] which complicates the separation of elastin and these molecules.

All the preceding inconveniences explain why an endofluorescence protocol has not yet been applied in living animals. In this study, we were not able to record any significant signal under normal physiological conditions [see Fig. 2(a)].

Because of the high quantum yield of the SRB (~80%) and the fact that high-wavelength photons are less absorbed and diffused, we showed that high-quality images of elastic fibers can be acquired within less than a second at 200 μm depth [Fig. 4(a)]. These experimental conditions enable intravital imaging [Fig. 4(f)]. The 3-D image acquisition of organs having important movements such as large arteries, can be accomplished *in situ* or in seconds after the euthanasia of the animal [Figs. 4(a)–4(e)].

Our method minimizes preparation artifacts that can be seen in tissue sections and biopsies since organs remain in physiological conditions; also note that the morphological differences of the elastic fibers were observed on fixed tissues versus fresh samples.[36]

Finally, there is no detectable emission for wavelength below 560 nm enabling a multiple staining protocol; other intravital dyes in the blue/green range [Fig. 3(a)] or transgenic animals expressing[36] Green Fluorescent Protein (GFP) can be simultaneously used. SHG signal can also be acquired in parallel [Fig. 4(a)].

4.3 *Specificity of the Staining*

In connective tissues, elastic fibers usually show a cobweb structure[16] with a smaller diameter than collagen fibers. It is typically the structure stained by SRB in Fig. 2(c). The confusion with other fibrous structures such as type I and III collagen[20,21] (SHG active) is refuted by the absence of colocalization with the SHG signal [Fig. 2(c)].

Furthermore, SRB-stained structures in artery walls are morphologically similar to those described as elastic fibers.[16,25] In Fig. 4(d), the fenestrated structure stained by SRB and reported to be the external elastic lamina is seen as the limit between the media and the adventia, which is the only layer of the artery wall being described to be SHG active.[17] Both internal and external elastic laminas can be imaged with high resolution (Fig. 4).

Morphological observations in different tissues enable us to conclude that SRB stains specifically elastic fibers.

Colocalization experiments on tissue sections with an immunohistological staining method of elastic fibers were also performed on fixed thoracic aorta rings (Fig. 5). A strong colocalization was observed between the SRB staining and an immunostaining of the elastin.

5 Conclusion

The intravital staining of elastic fibers by SRB reported in this paper enables their observation at a micrometric scale in less than a second. Elastic fibers were imaged in connective tissues, muscle, and blood vessels in the living animal after an intravenous injection or a local deposit of the stain. The low toxicity of the SRB enables multiple injections in the same animal and may enable the follow-up of elastic fiber modifications in animal models of various diseases. The spectral properties of SRB favor the simultaneous observation of other structures using SHG or other vital dyes.

Our method opens new horizons for numerous biomedical applications, such as aging,[37] dermatology,[38,39] vascular medicine,[18] and oncology.[19] In the latter case, the effects of elastases and matrix metalloproteases released by tumor cells

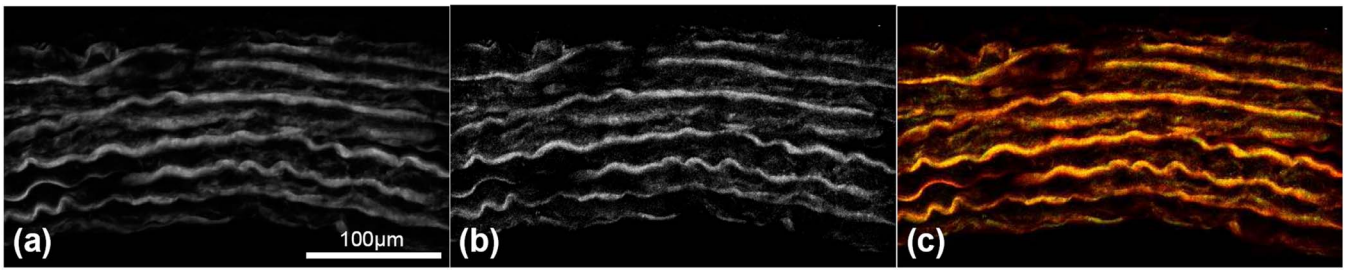

Fig. 5 Specificity of the staining: (a) cross section of a rat thoracic aorta stained with SRB, (b) the same section as (a) immunostained with an antielastin antibody, and (c) merge of the two previous pictures (SRB staining, red; immunolabelling, green). The colocalized areas appear in yellow. All of theses pictures are *z* projections of 10 images (spacing 1 μm) acquired using an 800-nm excitation wavelength with a 60-mW incident laser power. A rolling ball background subtraction with a radius of 50 pixels was applied on every picture before the *z* projection. (Color online only.)

could be observed directly *in vivo* and improve our knowledge on invasive tumor growth and metastasis.[40]

References

1. C. M. Kielty, M. J. Sherratt, and C. A. Shuttleworth, "Elastic fibres," *J. Cell. Sci.* **115**, 2817–2828 (2002).
2. R. Ross, "The elastic fiber: a review," *J. Histochem. Cytochem.* **21**, 199–208 (1973).
3. L. Debelle, A. J. P. Alix, S. M. Wei, M.-P. Jacob, J.-P. Huvenne, M. Berjot, and P. Legrand, "The secondary structure and architecture of human elastin," *Eur. J. Biochem.* **258**, 533–539 (1998).
4. L. Debelle and A. M. Tamburro, "Elastin: molecular description and function," *Int. J. Biochem. Cell Biol.* **31**, 261–272 (1999).
5. R. E. Shadwick, "Mechanical design in arteries," *J. Exp. Biol.* **202**, 3305–3313 (1999).
6. F. Helmchen and W. Denk, "Deep tissue two-photon microscopy," *Nat. Methods* **2**, 932–940 (2005).
7. K. König, "Multiphoton microscopy in life sciences," *J. Microsc.* **200**, 83–104 (2000).
8. P. Vérant, R. Serduc, B. van der Sanden, C. Rémy, and J.-C. Vial, "A direct method for measuring mouse capillary cortical blood volume using multiphoton laser scanning microscopy," *J. Cereb. Blood Flow Metab.* **27**, 1072–1081 (2007).
9. C. Stosiek, O. Garaschuk, K. Holthoff, and A. Konnerth, "In vivo two-photon calcium imaging of neuronal networks," *Proc. Natl. Acad. Sci. U.S.A.* **100**, 7319–7324 (2003).
10. D. Stockholm, M. Bartoli, G. Sillon, N. Bourg, J. Davoust, and I. Richard, "Imaging calpain protease activity by multiphoton FRET in living mice," *J. Mol. Biol.* **346**, 215–222 (2005).
11. W. R. Zipfel, R. M. Williams, R. Christie, A. Y. Nikitin, B. T. Hyman, and W. W. Webb, "Live tissue intrinsic emission microscopy using multiphoton-excited native fluorescence and second harmonic generation," *Proc. Natl. Acad. Sci. U.S.A.* **100**, 7075–7080 (2003).
12. D. Kleinfeld, P. P. Mitra, F. Helmchen, and W. Denk, "Fluctuations and stimulus-induced changes in blood flow observed in individual capillaries in layers 2 through 4 of rat neocortex," *Proc. Natl. Acad. Sci. U.S.A.* **95**, 15741–15746 (1998).
13. R. Serduc, P. Verant, J. Vial, R. Farion, L. Rocas, C. Remy, T. Fadlallah, E. Brauer, A. Bravin, J. Laissue, H. Blattmann. and B. vd. Sanden, "In vivo two-photon microscopy study of short-term effects of microbeam irradiation on normal mouse brain microvasculature," *Int. J. Radiat. Oncol., Biol., Phys.* **64**, 1519–1527 (2006).
14. K. W. Dunn, R. M. Sandoval, K. J. Kelly, P. C. Dagher, G. A. Tanner, S. J. Atkinson, R. L. Bacallao, and B. A. Molitoris, "Functional studies of the kidney of living animals using multicolor two-photon microscopy," *Am. J. Physiol.: Cell Physiol.* **283**, 905–916 (2002).
15. A. Nimmerjahn, F. Kirchhoff, J. N. Kerr, and F. Helmchen, "Sulforhodamine 101 as a specific marker of astroglia in the neocortex in vivo," *Nat. Methods* **1**, 31–37 (2004).
16. T. Ushiki, "Collagen fibers, reticular fibers and elastic fibers. A comprehensive understanding from a morphological viewpoint," *Arch. Histol. Cytol.* **65**, 109–126 (2002).
17. T. Boulesteix, A.-M. Pena, N. Pagès, G. Godeau, M.-P. Sauviat, E. Beaurepaire, and M. C. Schanne-Klein, "Micrometer scale ex vivo multiphoton imaging of unstained arterial wall structure," *Cytometry* **69**, 20–26 (2005).
18. B. S. Brooke, A. Bayes-Genis, and D. Y. Li, "New insights into elastin and vascular disease," *Trends Cardiovasc. Med.* **13**, 176–181 (2003).
19. W. Hornebeck and F. X. Maquart, "Proteolized matrix as a template for the regulation of tumor progression," *Biomed. Pharmacother* **57**, 223–230 (2003).
20. R. M. Williams, W. R. Zipfel, and W. W. Webb, "Interpreting second-harmonic images of collagen I fibrils," *Biophys. J.* **88**, 1377–1386 (2005).
21. W. Mohler, A. C. Millard, and P. J. Campagnola, "Second harmonic generation imaging of endogenous structural proteins," *Methods* **29**, 97–109 (2003).
22. C. Xu and W. W. Webb, "Measurement of two-photon excitation cross sections of molecular fluorophores with data from 690 to 1050 nm," *J. Opt. Soc. Am.* **13**, 481–491 (1996).
23. S. Fery Forgues and D. Lavabre, "Are fluorescence quantum yields so tricky to measure? A demonstration using familiar stationery products," *J. Chem. Educ.* **76**, 1260–1264 (1999).
24. T. Karstens and K. Kobs, "Rhodamine B and rhodamine 101 as reference substances for fluorescence quantum yield measurements," *J. Phys. Chem.* **84**, 1871–1872 (1980).
25. D. W. Fawcett, *Bloom and Fawcett—A Textbook of Histology*, Chapman & Hall, New York, (1994).
26. B. Yu, K. H. Kim, P. T. So, D. Blankschtein, and R. Langer, "Evaluation of fluorescent probe surface intensities as an indicator of transdermal permeant distributions using wide-area two-photon fluorescence microscopy," *J. Pharm. Sci.* **92**, 2354–2365 (2003).
27. L. V. Johnson, L. V. Walsh, and L. V. Chen, "Localization of mitochondria in living cells with rhodamine 123," *Proc. Natl. Acad. Sci. U.S.A.* **77**, 990–994 (1980).
28. H. Baatz, M. Steinbauer, A. G. Harris, and F. Krombach, "Kinetics of white blood cell staining by intravascular administration of rhodamine 6G," *Int. J. Microcirc.: Clin. Exp.* **15**, 85–91 (1995).
29. T. J. Ffytche, J. S. Shilling, I. H. Chisholm, and J. L. Federman, "Indications for fluorescein angiography in disease of the ocular fundus: a review," *J. R. Soc. Med.* **73**, 362–365 (1980).
30. P. Skehan, R. Storeng, D. Scudiero, A. Monks, J. McMahon, D. Vistica, J. T. Warren, H. Bokesch, S. Kenney, and M. R. Boyd, "New colorimetric cytotoxicity assay for anticancer-drug screening," *J. Natl. Cancer Inst.* **82**, 1107–1112 (1990).
31. K. König, K. Schenke-Layland, I. Riemann, and U. A. Stock, "Multiphoton autofluorescence imaging of intratissue elastic fibers," *Biomaterials* **26**, 495–500 (2005).
32. K. Schenke-Layland, I. Riemann, U. A. Stock, and K. Konïg, "Imaging of cardiovascular structures using near-infrared femtosecond multiphoton laser scanning microscopy," *J. Biomed. Opt.* **10**, 024017 (2005).
33. S.-J. Lin, R.-J. Wu, H.-Y. Tan, W. Lo, W.-C. Lin, T.-H. Young, C.-J. Hsu, J.-S. Chen, S.-H. Jee, and C.-Y. Dong, "Evaluating cutaneous photoaging by use of multiphoton fluorescence and second-harmonic generation microscopy," *Opt. Lett.* **30**, 2275–2277 (2005).
34. A. Zoumi, X. Lu, G. S. Kassab, and B. J. Tromberg, "Imaging coronary artery microstructure using second-harmonic and two-photon

fluorescence microscopy," *Biophys. J.* **87**, 2778–2786 (2004).
35. D. Débarre, W. Supatto, A.-M. Pena, A. Fabre, T. Tordjmann, L. Combettes, M.-C. Schanne-Klein, and E. Beaurepaire, "Imaging lipids bodies in cells and tissues using third-harmonic generation microscopy," *Nat. Methods* **3**, 47–53 (2006).
36. Y. C. Fung and S. S. Sobin, "The retained elasticity of elastin under fixation agents," *J. Biomed. Eng.* **103**, 121–122 (1981).
37. L. Robert, "Mechanisms of aging of the extracellular matrix: role of the elastin-laminin receptor," *Gerontology* **44**, 307–317 (1998).
38. K. G. Lewis, L. Bercovitch, S. W. Dill, and L. Robinson-Bostom, "Acquired disorders of elastic tissue: part 1. Increased elastic tissue and solar elastotic syndromes," *J. Am. Acad. Dermatol.* **51**, 1–21 (2004).
39. K. Schenke-Layland, I. Riemann, O. Damour, U. A. Stock, and K. Konïg, "Two-photon microscopes and in vivo multiphoton tomographs—powerful diagnostic tools for tissue engineering and drug delivery," *Adv. Drug Delivery Rev.* **58**, 878–896 (2006).
40. K. Lapis and J. Timar, "Role of elastin-matrix interactions in tumor progression," *Semin Cancer Biol.* **12**, 209–217 (2002).